Nonequilibrium Viscous Shock-Layer Technique for Hypersonic Blunt-Nosed Slender Bodies

S. Ghasemloo, M. Main and S. Noori

Amirkabir University of Technology, Tehran, Iran, 15875-4413

Center of Excellence in Computational Aerospace Engineering

Abstract

A nonequilibrium viscous shock layer solution procedure is presented that considerably improves the computational efficiency, especially for long slender bodies. The present approach generates its own shock shape as a part of solution and provides a smooth shock shape in subsonic and supersonic regions. In the nose region, shock shape is specified from an algebraic expression and corrected through global passes through that region. The shock shape is computed as part of the solution beyond the nose region and requires only a single global pass. For this study, a seven-species $(O_2, N_2, O, N, NO, NO^+, e^-)$ air model is used. The chemical reaction model is taken from Blottner. The method of solution is a spatial marching, implicit, finite difference technique, which includes coupling of the normal momentum and continuity equations. The computational results obtained show good agreement compared to the STS-2 flight data and other numerical solutions.

Nomenclature

c_i	mass fraction of species i, ρ_i / ρ	u	velocity component tangent to the shock, u^*/V_∞^*
c_p	specific heat at constant pressure, $c_P^*/c_{P\infty}^*$	v	velocity component normal to the shock, u^*/V_∞^*
h	static enthalpy, h^*/V_∞^2	ε	Reynolds number parameter, $(\mu_{ref}/\rho_\infty^* u_n^* R_n^*)^{1/2}$
h_1, h_3	metrics	Γ_b	body angle
J_i	diffusion mass flux of species i, $J_i^* R_n^*/\mu_{ref}$	η_n	normalized n coordinate, 1-n/n_b
k	thermal conductivity, $k^*/\mu_{ref}^* C_{P\infty}^*$	μ	viscosity, u^*/μ_{ref}^*
$k_{i,w}$	surface reaction rate coefficient, $k_{i,w}^*/V_\infty$	ξ	normalized s coordinate, ξ = s
Le	Lewis number	ρ	density, ρ^*/ρ_∞
M	Mach number	γ	catalytic recombination coefficient of species *i*
M_i	molecular weight of species i	$\dot{\omega}$	mass rate of formation of species i, $\dot{\omega}^* R_n^*/\rho_\infty^* V_\infty^*$
R_n	body nose radius		
R_u^*	universal gas constant		**Subscript and superscript**
r	radius measured from axis of symmetry, r^*/R_n^*	i	species index
s	coordinate measured along the shock wave, s^*/R_n^*	w	wall value
T	temperature, $T^* C_{P\infty}^*/V_\infty^2$	∞	free stream condition
y	distance normal to body	*	dimensional quantities

1. Introduction

The return of space vehicles to the earth's surface with their structure intact is one of the most important problem in design of these vehicles. During reentry of a space vehicle through the atmosphere , extremely high velocities are encountered. At the high speeds that a vehicle reenters the atmosphere , the temperature near the body becomes extremely high, especially in the stagnation region. The high temperature and high convective velocities relative to reaction times create an environment where chemical nonequilibrium effects can be significant. Therefore, the air in the shock layer dissociates and ionizes. These phenomena will change considerably the chemical composition of the air and this change will extended along the body. Accurate aerothermodynamic predictions during this part of the reentry trajectory are essential for sizing the thermal protection system. For an accurate description of the flowfield, one must account for these real gas effects. Also an accurate estimate of the ionization level is needed for radio communication purposes. Therefore, a flowfield model including finite rate chemistry is require. For many hypersonic applications, forebody configurations are relatively simple and can be modeled by long slender bodies of revolution with a blunted nose. The calculation of hypersonic viscous flowfields past long slender axisymmetric blunt bodies is of prime interest to the designer of certain aerospace vehicles. Since simulation of the high-energy thermodynamic environment of earth entries in ground–based experimental facilities is difficult, accurate and reliable flowfield prediction capabilities must be developed for efficient and reliable design of reentry vehicle. Three popular computational approaches for obtaining aerothermodynamics predictions on these classes of vehicles are to solve the Navier-Stocks(NS) equations[1], Parabolized Navier-Stokes(PNS) equations[2] or Viscous Shock-Layer (VSL) equations. For highest fidelity, solutions to the full Navier–Stokes equations would be required , but this is very time- consuming both in human labor as well as computer time and not well suited for practical design and analysis study. The PNS equations can be solved using a space marching technique instead of the time marching procedure which is usually employed for the NS equations. The principle difficulty in applying the PNS equations to the hypersonic vehicles is that commonly the algorithms cannot solve blunt–body flowfields, while most reentry vehicle designs incorporate blunted nose in order to reduce peak heating rates. In addition, the numerical solution of the PNS equations requires a substantial amount of computer time and storage. The extensive computer run times prevent these approaches (i.e. NS and PNS) from being used in the preliminary design environment.

The third approach is to employ the Viscous Shock–Layer (VSL) equations. The VSL equations were developed by Davis [3] and yield a simplified set of governing equations that are uniformly valid through the shock layer. The VSL method can accurately predict the blunt-body flowfield for a small fraction of the computing time required by NS schemes. This choice is very desirable for the preliminary design process where a range of geometries and flow parameters must be analyzed.

Blottner [4] was the first to develop the VSL approach for a multicomponent reacting gas at the stagnation point. He was followed shortly thereafter by R.T. Davis, who solved the VSL equations for a binary reacting gas and included flow downstream of the stagnation point [5]. Both these works treated the fully catalytic case. Miner and Lewis [6] extended the method of Davis to a seven-species mixture and applied both fully catalytic and noncatalytic boundary conditions. Scott [7] modified the Miner and Lewis code to include finite-rate catalycity for oxygen and nitrogen recombination. Lewis et al developed a three-dimensional VSL code for non equilibrium flow over the Space Shuttle [8] and included surface catalytic effects [9]. Based on_Davis analysis, Moss [10] developed a code using the VSL equations for a multicomponent gas mixture with chemical equilibrium or nonequilibrium. The VSL method of Ref.10 updated [11] by coupling the normal momentum and continuity equations, which made the method of Ref. 10 stable even for the massive blowing conditions.

In the previous methods, an initial shock shape was required to start the solution of VSL equations. This was obtained by various procedures, each requiring considerable computational effort. Moreover, the shock shape extending to the entire length of the body is globally iterated. The initial shock shape generation and the global iterations over the entire length of the body required considerable computational effort and run time respectively. Riley [12] developed a method to obtain the inviscid flowfield around the blunt bodies in which the shock shape was generated. Cheatwood [13] used the same method to solve the Approximate Viscous Shock Layer (AVSL) equations. In the present work, this method was developed for solving the VSL equations in chemical

nonequilibrium flow conditions**.** The present approach generates its own shock shape as a part of solution and provides a smooth shock shape in subsonic and supersonic regions. Therefore, the input shock shape obtained from a different solution is not required. It eliminates the need for initial shock shape, which was required by previous method of solutions. Moreover, the global iterations are limited to the subsonic region which is small region in the hypersonic flow over the blunt bodies. The VSL equations are solved in a shock oriented (rather than the traditional body oriented) coordinate system. Note that the use of a body coordinate system introduces discontinuities in the solution of governing equations associated with the surface curvature discontinuity, such as at the sphere–cone tangency point of a spherically blunted cone. Also, the first-order continuity and normal momentum equations are solved simultaneously and the Vigneron condition is employed for the streamwise pressure gradient in the subsonic nose region. For most reentry applications, the temperature in the shock layer is such that a seven-species reacting model with a single ionizing species represents the chemistry reasonably well. In the present work, seven species ionizing air is considered, and it is assumed that chemical reactions proceed at finite rate. The accuracy of the developed code is validated by comparing the computational results with other solutions and available experimental data.

2. Governing Equations

The conservation equations employed in this analysis are the viscous shock-layer equations for a blunt axisymmetric body at zero angle of attack. These equations are written in a shock oriented coordinate system (s,n) where the s coordinate is tangent to the shock in the stream wise direction and n is the normal to the shock (see Figure 1). To Facilitate the solution, the VSL equations are transformed to normalized coordinates (ξ,η_n). The nondimensional forms of the VSL equations for nonequilibrium flow in a normalized shock oriented coordinate system are:
global continuity :

$$\frac{\partial}{\partial\xi}(\rho u h_3)-\frac{dn_b}{d\xi}\frac{\eta_n-1}{n_b}\frac{\partial}{\partial\eta_n}(\rho u h_3)-\frac{1}{n_b}\frac{\partial}{\partial\eta_n}(\rho v h_1 h_3)=0 \tag{1}$$

ξ-momentum:

$$\begin{aligned}&\rho[\frac{u}{h_1}(\frac{\partial u}{\partial\xi}-\frac{\eta_n-1}{n_b}\frac{dn_b}{d\xi}\frac{\partial u}{\partial\eta_n})-\frac{v}{n_b}(\frac{\partial u}{\partial\eta_n}+\frac{u}{h_1}\frac{\partial h_1}{\partial\eta_n})]+\frac{1}{h_1}(\frac{\partial p}{\partial\xi}-\frac{\eta_n-1}{n_b}\frac{dn_b}{n\xi}\frac{\partial p}{\partial\eta_n})\\&=\frac{\varepsilon^2}{n_{b^2}}\{\frac{\partial}{\partial\eta_n}[\mu(\frac{\partial u}{\partial\eta_n}-\frac{u}{h_1}\frac{\partial h_1}{\partial\eta_n})]+\mu(\frac{2}{h_1}\frac{\partial h_1}{\partial\eta_n}+\frac{1}{h_3}\frac{\partial h_3}{\partial\eta_n})(\frac{\partial u}{\partial\eta_n}-\frac{u}{h_1}\frac{\partial h_1}{\partial\eta_n})\}\end{aligned} \tag{2}$$

n-momentum:

$$\rho n_b[\frac{u}{h_1}\frac{\partial v}{\partial\xi}-(\frac{v}{n_b}+\frac{u}{h_1}\frac{\eta_n-1}{n_b}\frac{dn_b}{d\xi})\frac{\partial v}{\partial\eta_n}+\frac{u^2}{h_1 n_b}\frac{\partial h_1}{\partial\eta_n}]-\frac{\partial p}{\partial\eta_n}=0 \tag{3}$$

Energy:

$$\begin{aligned}&\rho C_{pf}[\frac{u}{u_1}(\frac{\partial T}{\partial\xi}-\frac{\eta_n-1}{n_b}\frac{dn_b}{d\xi}\frac{\partial T}{\partial\eta_n})-\frac{v}{n_b}\frac{\partial T}{\partial\eta_n}]-\frac{u}{h_1}(\frac{\partial p}{\partial\xi}-\frac{\eta_n-1}{n_b}\frac{dn_b}{n\xi}\frac{\partial p}{\partial\eta_n})\\&+\frac{v}{n_b}\frac{\partial p}{\partial\eta_n}=\frac{\varepsilon^2}{n_{b^2}}\{\frac{\partial}{\partial\eta_n}k(\frac{\partial T}{\partial\eta_n})+k\frac{\partial T}{\partial\eta_n}(\frac{1}{h_1}\frac{\partial h_1}{\partial\eta_n}+\frac{1}{h_3}\frac{\partial h_3}{\partial\eta_n})+\mu(\frac{\partial u}{\partial\eta_n}-\frac{u}{h_1}\frac{\partial h_1}{\partial\eta_n})^2\}\\&+\frac{\varepsilon^2}{n_{b^2}}\frac{\mu Le_{12}}{p_r}\sum_{i=1}^{Ns}Cp_i\frac{\partial c_i}{\partial\eta_n}\frac{\partial T}{\partial\eta_n}-\sum_{i=1}^{Ns}h_i\dot{\omega}_i\end{aligned} \tag{4}$$

Species Continuity:

$$\rho[\frac{u}{h_1}(\frac{\partial c_i}{\partial\xi}-\frac{\eta_n-1}{n_b}\frac{dn_b}{d\xi}\frac{\partial c_i}{\partial\eta_n})-\frac{v}{n_b}\frac{\partial c_i}{\partial\eta_n}]=\dot{\omega}_i+\frac{\varepsilon^2}{{n_b}^2 h_1 h_3}\frac{\partial}{\partial\eta_n}(h_1 h_3\frac{\mu Le_{12}}{p_r}\frac{\partial c_i}{\partial\eta_n}) \tag{5}$$

State:

$$P = \rho R_u T \sum_{i=1}^{Ns} \frac{c_i}{Mi} \tag{6}$$

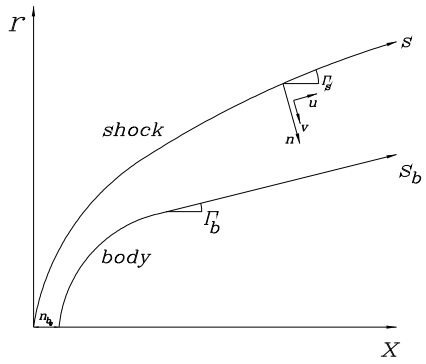

Figure 1: Shock-oriented coordinate system

3. Boundary Conditions

The boundary conditions at the shock are obtained by using the Rankine-Hugoniot relations. The flow behind the shock is assumed to be frozen at the freestream composition. No slip boundary conditions are employed at the surface because the VSL equations in this study are used only at lower altitudes. The wall conditions of chemical species are governed by catalytic relations on the wall and are obtained from the equation :

$$J_{i,w} - \frac{\rho k_{i,w}}{\varepsilon^2} c_i = 0 \tag{7}$$

In the present work, three catalytic wall boundary conditions namely noncatalytic wall, fully catalytic wall, and finite rate catalytic wall are used. For a noncatalytic wall, the catalytic recombination rate is equal to zero [14], i.e.

$$\left(\frac{\partial c_i}{\partial \eta_n} \right) = 0 \tag{8}$$

On the fully catalytic wall, the gas species are assumed to recombine to the freestream composition, i.e.

$$c_{i,w} = c_{i,\infty} \tag{9}$$

For the finite catalytic wall, the catalytic recombination rate is expressed as

$$k_{i,w} = \sqrt{\frac{R_u^* T_w^*}{2\pi M_i^*}} \gamma_i \tag{10}$$

In the present study, according to Ref.[15], the recombination coefficient for oxygen atom γo is given as

$$\gamma_O = 8.0 \exp(-8600 / T_w^*) \tag{11}$$

The recombination coefficient for nitrogen is the same as that employed by Scott [16]:

$$\gamma_N = 0.00714 \exp(-2219 / T_w^*) \tag{12}$$

4 Thermodynamic and Transport Properties

In the present work, as mentioned earlier, a seven-species nonequilibrium chemistry model was employed. Thermodynamic properties for specific heat and enthalpy and transport properties for viscosity and thermal conductivity are required for each species considered. Values for the thermodynamic and transport properties are obtained by using curve fits explain in [17]. The mixture viscosity is obtained by using the Wilke's semi-imperical relation [18], and the mixture thermal conductivity is calculated using the formula of Mason and Saxena [19]. A constant Lewis number of 1.4 is used, and a variable Prandtle number is computed.

5. Shock Shape

The VSL equations require an initial shock shape for the first global iteration. The shock shape obtained in the first iteration solution is used as the input shape for a second iteration. This procedure is repeated until the new calculated shock shape varies little from the input shape. Most of existing VSL schemes use the various procedures (thin viscous shock layer, inviscid solution,…) to obtain an initial shock shape. However, obtaining the initial shock shape from these procedures require considerable computational effort. In the present approach, the shock shape is generated as part of the solution. The shock shape is calculated based upon the method which is presented in Ref. [12]. As mentioned earlier, the subsonic-transonic region is elliptic in nature, therefore, a marching scheme is not well posed. Thus, the complete shock shape for the entire subsonic-transonic region must be determined iteratively. A marching procedure is then used downstream of the subsonic-transonic region where the inviscid layer is supersonic. Generally, the three-dimensional shock surface in the subsonic-transonic region can be represented by three longitudinal conic sections blended in the circumferential direction with an ellipse [12].The equation of the longitudinal conic sections is given by

$$f_k^2 + b_k x^2 - 2c_k x + 2d_k x f_k = 0 \ , k = 1,2,3 \tag{13}$$

Note that $F(x,\phi)$ is the radial coordinate of the 3D shock surface in shock cylindrical coordinate system.Where k represents shock profiles for ϕ=0°, 90° and 180°, respectively. The shock shape, defined above includes nine parameters of b_k, c_k and d_k where k=1,2,3. For an axisymmetric flow, the total number of parameters governing the shock surface is reduced to b_1 and c_1 [12]. The quantities b_1 and c_1 are determined through a quasi-Newton iterative procedure. With each variation of these two parameters, the flowfield is solved for the entire subsonic region. The values for the calculated shock layer thickness at two stations near the end of the subsonic region are compared with the values imposed by the geometry. Shock iterations are continued until the calculated values of nb at these two stations match to the geometric values. Downstream the subsonic-transonic region, the initial shock shape is calculated by linear extrapolation of previous values and is corrected iteratively using the secant method. It is to be noted that the shock shape convergence is achieved with four to six iterations per station. As an initial value, the curvature at station i is extrapolated from its values at the previous two stations. Once the shock geometry and the corresponding jump conditions are constrained, the governing equations are solved. Then the calculated and geometric values of n_b are compared to determine the error (δerr). Through successive application of the secant method (accompanied by a solution to the fluid equations), δerr converges to a specified tolerance. In summary, in the subsonic-transonic region, shock shape is specified from an algebraic relation and corrected through global iterations through that region. The shock shape is computed as part of the solution beyond the subsonic-transonic region. Thus, shock shape is not required as an input by the user.

6. Method of Solution

The method used for solving the full VSL equations is a spatial-marching, implicit, finite-difference method which includes coupling of the continuity and normal momentum equations. In the normalized shock-coordinate system (ξ, η_n), the conservation equation for streamwise momentum and energy can be written in the standard parabolic form:

$$A_0 \frac{\partial^2 W}{\partial \eta_n^2} + A_1 \frac{\partial W}{\partial \eta_n} + A_2 W + A_3 + A_4 \frac{\partial W}{\partial \xi} = 0 \tag{14}$$

Where W represents the dependents variables u, T and, c_i respectively. The coefficients A_0 through A_4 are nonlinear coefficients. For the energy equation, the nonlinearities are handled through a simple lagging technique. However, in order to speed convergence, the streamwise momentum equation is quasi-lineralized. In the finite-difference method used to solve the streamwise and energy equations, a two point backward differences is used for the derivatives with respect to ξ. The derivatives with respect to the η_n are replaced with three-point central differences. Replacing the differential terms by the finite-difference expressions, the governing equations are expressed as:

$$A_j W_{i,j-1} + B_j W_{i,j} + C_j W_{i,j+1} = D_j \tag{15}$$

Evaluating the coefficients of Eq. (15) at discrete points across the shock layer along with the boundary conditions yields a tri-diagonal system of equations which may be solved using Thomas algorithm. The continuity and normal momentum equations are first order differential equations and, when solved independently, pose numerical difficulties. However, using the coupling approach, these two first equations are coupled together to form a second-order system that can be solved using Thomas algorithm. These equations are solved for the pressure and normal velocity. The density in these equations is eliminated by using the equation of state. The resulting equations are expressed in the finite-difference form at points (i,j+½) and (i,j-½) using a box scheme. The final form for the continuity and normal momentum equations are :

$$\begin{aligned}
&A_{c,j+1/2} V_{i,j+1} + B_{c,j+1/2} V_{i,j} + C_{c,j+1/2} P_{i,j+1} + D_{c,j+1/2} P_{i,j} = E_{c,j+1/2} \\
&A_{c,j-1/2} V_{i,j} + B_{c,j-1/2} V_{i,j-1} + C_{c,j-1/2} P_{i,j} + D_{c,j-1/2} P_{i,j-1} = E_{c,j-1/2} \\
&A_{nm,j+1/2} V_{i,j+1} + B_{nm,j+1/2} V_{i,j} + C_{nm,j+1/2} P_{i,j+1} + D_{nm,j+1/2} P_{i,j} = E_{nm,j+1/2} \\
&A_{nm,j-1/2} V_{i,j} + B_{nm,j-1/2} V_{i,j-1} + C_{nm,j-1/2} P_{i,j} + D_{nm,j-1/2} P_{i,j-1} = E_{nm,j-1/2}
\end{aligned} \tag{16}$$

Eliminating p and v alternatively in the coupled equations, two tridiagonal equations for pressure and normal velocity are obtained as:

$$A_p p_{i,j-1} + B_p p_{i,j} + C_p p_{i,j+1} = D_p \tag{17}$$

$$A_v v_{i,j-1} + B_v v_{i,j} + C_v v_{i,j+1} = D_v \tag{18}$$

Equations (17) and (18) are solved in the same way as the streamwise momentum, energy and species continuity equations. This numerical coupling enhances considerably the overall numerical stability of the VSL solution scheme. It is note to be that the shock standoff distance is evaluated by integrating the continuity equation.

The solution is started at the stagnation line. Using the stagnation line solution, the VSL equations are solved at the next down stream location by employing a two point backward-difference approximation for the streamwise derivative. The solution is iterated until the convergence is achieved. This procedure is repeated until a global solution at all locations is obtained. Note that the rate of production terms which are function of both T and c_i, appears in the species conservation and energy equations. For the species conservation equations, Blottner's approach is used to linearize the production terms such that the species conservation appears as the only unknown. Furthermore, the production terms in the energy equation are also linearized such that the temperature appears as the only unknown. It is mentioned that at each location the equations are solved in the following order: The species conservation, energy and streamwise momentum equation are solved for c_i, T and u, respectively. The integration of

the continuity equation determines the shock layer thickness, n_b. Then, the continuity and normal momentum equations are solved simultaneously for p and v. Finally, the density ρ is obtained using the equation of state.

7. Results and Discussion

In this section of the paper, the results of the present method are compared with existing results. Figures 2 and 3 represent the result of the application of the method to STS-2 laminar heating and the results from the experiments from Ref.[20]. An "equivalent axisymmetric body" concept was used in Ref.[20] to model the windward centerline of the shuttle at a given angle of attack with an appropriate axisymmetric body at zero angle of attack. The axisymmetric body is hyperboloid with nose radii R_n and asymptotic body half-angles Γ_b as given in each figure. The results that are shown on each figure are the experimental data and present VSL predictions based on a finite catalytic wall condition using k_w, based on Eq. (10). In Figure 2, the surface heating rate for an altitude of 77.91 km are presented and are seen to compare well (generally within twenty percent) with the experimental data. At 60.56 km altitude (Figure 3), the agreement between the predicted and measured heating value is quite good (within five percent). The heating rates of present method for 6 and 20 deg sphere cones are compared with the VSL method by Lee [11] in Figures 4-5. Freestream conditions are for 53.34 km altitude and Mach number of 25.The bodies have the same nose radius which equals 0.0381m. Both noncatalytic and fully catalytic surface are examined to show the limiting effects of wall catalycity on heating. It should be mentioned that all calculations were done using 101 grid points between the body and the shock. The results of present method are generally in good agreement (within four to fifteen percent) with the Lee method. The computed heating rate for 6˚ sphere-cone show excellent agreement with the results by Lee. While the 20˚ sphere-cone shows a greater deviation. However, the maximum deviation (in the spherical region) was found to be fifteen percent. From these figures, it is seen that the heating rates with the noncatalytic surface may decrease more than 45% in comparison to that with the fully catalytic surface on the spherical region. The differences in the heating rates decrease in the downstream region. Since globally iterated results have been demonstrated to be quite accurate [11], results obtained by the present method are also considered equally good. The shock standoff distance for a 10˚ sphere-cone is shown in Figure 6. The results obtained from the present method are in good agreement with those obtained from the globally iterated technique. The electron concentration profiles for the RAM C 9˚ sphere-cone are shown in Figure. 7. Predictions of electron concentration profiles for S_b =8.8 are given for 70.104, 76.20, 80.772 and 83.820 km. The freestream velocity and wall temperature for these altitudes are 7620m/s and 1000˚k, respectively. In Figure 7, the calculated results are compared with the experimental data [21]. The present calculations agree reasonably well with the experimental data as to level of ionization. The agreement between the present predictions and the experimental data is good at 70.104, 76.20 and 80.772 km, but at 83.82km, the present method significantly underpredicted electron concentration. It is important to notice that the present results are for no slip conditions. It seems using the slip boundary condition will improve the results especially for altitude of 83.82 km. From these figures, it is concluded that the results of the present method are enough accurate against the results of experiments and other methods of solution.

8. Conclusions

A new technique to solve nonequilibrium viscous shock layer equations is proposed with increases computational efficiency. For this study, a seven-species air model is used and the chemical reaction model is taken from Blottner. In the present method, initial shock shape is not required and the global iteration is confined merely to nose region. The shock shape is defined with an algebraic (conic) equation and is iterated globally in the nose region till the calculated body matches with the real body at the end of the subsonic region. In the supersonic region, the marching scheme is well posed. Hence, the shock shape and flow field can be determined in each station and there is no need for global iteration. Since the subsonic region is only a small portion of the flow field for hypersonic flows over slender bodies, and the global iteration is confined for this region only in the present method, a dramatic reduction in CPU time is achieved. Moreover, by using the shock coordinated systems the junction point problem in sphere-cone

configurations is solved. Results of the present method compare quite favorably with experimental data and other predictions.

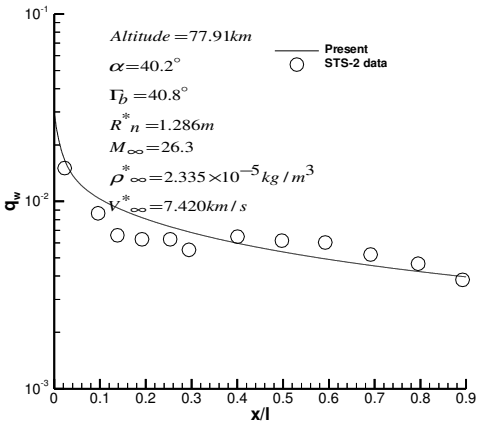

Figure 2: Comparison of calculated and measured heating rates an altitude of 77.91 km.

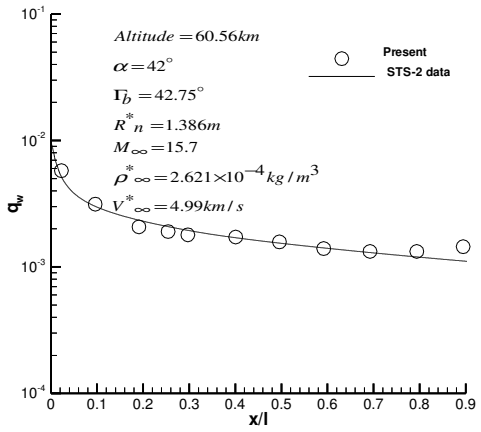

Figure 3: Comparison of calculated and measured heating rates an altitude of 60.56 km.

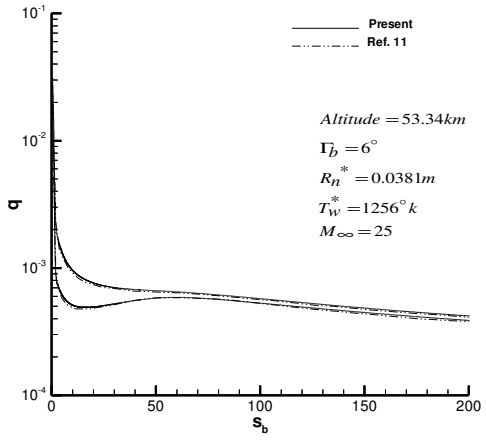

Figure 4: Nonequilibrium heating rate comparison for 6º sphere-cone.

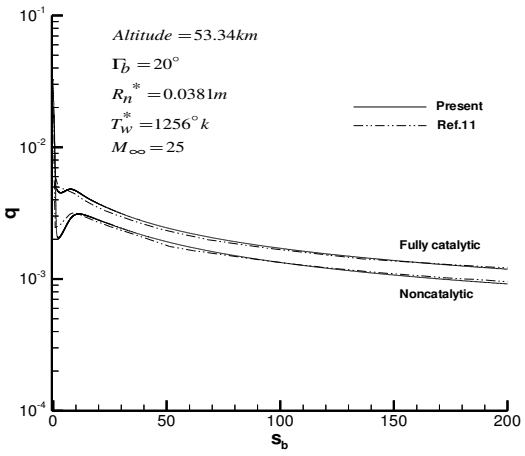

Figure 5: Nonequilibrium heating rate comparison for 20º sphere-cone.

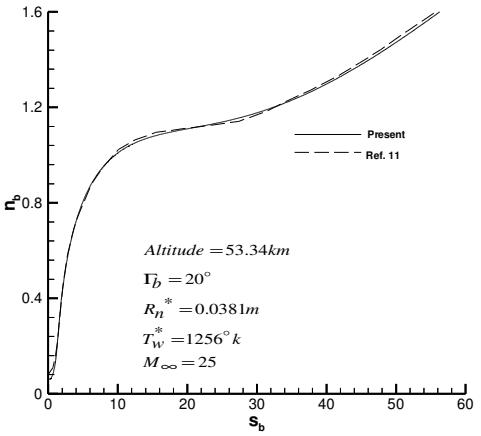

Figure 6: Shock standoff distance comparison for 20º sphere-cone with nonequilibrium chemistry.

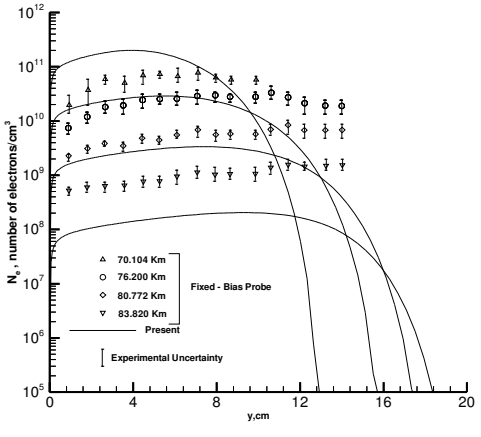

Figure 7: Comparison of electron concentration profiles for RAM C .

References

[1] Olynick D.R. and Tiwari S.B. Navier-Stokes Heating calculations for Benchmark Thermal Protection System Sizing . *J.Spacecraft and Rockets*, Vol. 33, No. 6, 1996, pp. 807-814.

[2] Bhutta B.A. and Lewis C.H. Comparison of Hypersonic Experiments and PNS predictions. *J.Spacecraft and Rockets*, Vol. 28, No. 4, 1991, pp. 376-386.

[3] Davis R.T. Numerical Solution of the Hypersonic Viscous Shock Layer Equatons. *AIAA J.*, Vol. 8, No. 5, 1970, pp. 843-851.

[4] Blottner F.G. Viscous Shock Layer at the Stagnation Point with Nonequilibrium Air chemistry. *AIAA J.*, Vol. 7, No. 12, Dec. 1969, pp. 2281-2287.

[5] Davis R.T. Hypersonic Flow of a Chemically Reacting Binary Mixture Past a Blunt Body. AIAA-70-805, 1970.

[6] Miner E.W. and Lewis C.H. Hypersonic Ionizing Air Viscous Shock-Layer Flows Over Nonanalytic Blunt Bodies. NASA CR-2550, 1975.

[7] Scott C.D. Effects of Nonequilibrium and Wall Catalysis on Space Shuttle Heat Transfer. *J. Spacecraft and Rockets*, Vol. 22, 1985, pp. 489-499.

[8] Kim M.D. , Swaminathan S., and Lewis C.H. Three Dimensional Nonequilibrium Viscous Flow Over the Space Shuttle Orbiter. *J. Spacecraft and Rockets*, Vol. 21, 1984, PP. 29-35.

[9] Kim M.D., Swaminathan S. and Lewis C.H. Three Dimensional Viscous Flow Over the Shuttle With Surface Catalytic Effects. AIAA-83-1426,1983.

[10] Moss J.N. Reacting Viscous Shock Layer Solutions With Multicomponent Diffusion and Mass Injection. NASA TR-R-411, 1974.

[11] Lee K.P. and Gupta R.N. Viscous Shock-Layer Analysis of Hypersonic Flows Over Long Slender Vehicles. NASA CR-189614, 1992.

[12] Riley C.J. An Engineering Method for Interactive Inviscid-Boundary Layers in Three-Dimensional Hypersonic Flows. PH.D Thesis, North Carolina State University, 1992.

[13] Cheatwood F.M. and DeJarnette F.R. An Approximate Viscous shock Layer Technique for Calculating Nonequilibrium hypersonic Flows About Blunt-Nosed Bodies. AIAA-92-0498,1992.

[14] Gupta R.N., Scott C.D., and Moss J.N. Slip-Boundary Equations for Multicomponent Nonequilibrium Airflow. NASA TP-2452, November 1985.

[15] Gupta R.N. Reevaluation of Flight-Derived Surface Recombination-Rate Expression for Oxygen and Nitrogen. *J. Spacecraft and Rockets*, Vol. 33, No. 3, 1996, pp. 451-453.

[16] Scott C.D. Catalytic Recombination of Oxygen and Nitrogen in High Temperature Reusable Surface Insulation. Aerothermodynamics and Planetary Entry, edited by A.L. Crosbie, Vol. 77, Progress in astrodynamics and Aeronautics, AIAA, New York, 1981, pp. 192-212.

[17] Thompson R.A., Lee K.P., and Gupta R.N. Computer Codes for The Evaluation of Thermodynamic Properties, Transport Properties, and Equilibrium Constants of an 11-Species Air Model. NASA TM-102602, February 1990.

[18] Wilke C.R. A Viscosity Equation for Gas Mixtures. *Journal of Chimical Physics*, Vol. 18, No. 4, 1950, pp. 517-519.

[19] Mason E.A., and Saxena S.C. Approximate Formula for the Thermal Conductivity of Gas Mixtures. The Physic of Fluids, Vol. 3, No. 5, 1958, pp. 361-369.

[20]Shinn J.L., Moss J.N. and Simmonds A.L. Viscous-Shock-Layer Heating Analysis for the Shuttle Windward Plane With Surface Finite Catalytic Recombination Rates. AIAA-82-0842, 1982.

[21]Evans J.S., Schexnayder C. J., Jr., and Huber P.W. Boundary-Layer Electron Profiles for Entry of a Blunt Slender Body at High Attitude. NASA TN D-7332, July 1973.

This page has been purposedly left blank